Annual Reviews in Control 41 (2016) 58–70

Contents lists available at ScienceDirect

Annual Reviews in Control

journal homepage: www.elsevier.com/locate/arcontrol

Comparison of closed-loop system identification techniques to quantify multi-joint human balance control

D. Engelhart[a,*], T.A. Boonstra[a], R.G.K.M. Aarts[b], A.C. Schouten[a,c], H. van der Kooij[a,c]

[a] Department of Biomechanical Engineering, University of Twente, MIRA institute for biomechanical technology and technical medicine, Enschede,7500 AE, The Netherlands
[b] Department of Mechanical Automation, University of Twente, Enschede, 7500 AE, The Netherlands
[c] Department of Biomechanical Engineering, Delft University of Technology, 2628 CD Delft, The Netherlands

ARTICLE INFO

Article history:
Received 16 June 2015
Revised 10 January 2016
Accepted 15 February 2016
Available online 4 May 2016

Keywords:
Balance control
Multiple-input multiple-output
Closed-loop
System identification

ABSTRACT

The incidence of impaired balance control and falls increases with age and disease and has a significant impact on daily life. Detection of early-stage balance impairments is difficult as many intertwined mechanisms contribute to balance control. Current clinical balance tests are unable to quantify these underlying mechanisms, and it is therefore difficult to provide targeted interventions to prevent falling. System identification techniques in combination with external disturbances may provide a way to detect impairments of the underlying mechanisms. This is especially challenging when studying multi-joint coordination, i.e. the contribution of both the ankles and hips to balance control.

With model simulations we compared various existing non-parametric and parametric system identification techniques in combination with external disturbances and evaluated their performance. All methods are considered multi-segmental (both the ankles and the hips contribute to maintaining balance) closed-loop balance control. Validation of the techniques was based on the prediction of time series and frequency domain data. Parametric system identification could not be applied in a straightforward manner in human balance control due to assumed model structure and biological noise in the system. Although the time series were estimated reliably, the dynamics in the frequency domain were not correctly estimated. Non-parametric system identification techniques did estimate the underlying dynamics of balance control reliably in both time and frequency domain. The choice of the external disturbance signal is a trade-off between frequency resolution and measurement time and thus depends on the specific research question and the studied population.

With this overview of the applicability as well as the (dis)advantages of the various system identification techniques, we can work toward the application of system identification techniques in a clinical setting.

1. Introduction

Maintaining a stable upright posture is a complex task. The body is inherently unstable due to the gravitational pull, and it would fall without stabilizing control. The central nervous system (CNS) stabilizes the body by integrating sensory feedback signals to determine the appropriate response, which is sent to the muscles and results in corrective joint torques to keep the body upright (Peterka, 2003). How the stabilizing mechanism of the CNS regulates balance can be investigated by estimating the dynamics of the so-called neuromuscular controller that outputs corrective joint torques as a response to body sway (Engelhart et al., 2014).

With aging or due to disease, sensory systems or the neuromuscular controller can deteriorate and as a result, balance control problems can arise (Pasma et al., 2014). For example, the elderly often have difficulties maintaining balance during daily life activities, and this impaired balance is a strong risk factor for falls (Rubenstein, 2006; Muir, Berg, Chesworth, Klar, & Speechley, 2010). About 28–35% of people aged over 65, fall each year and this incidence increases with age (WHO, 2007). To determine who is at risk of falling, clinicians use clinical balance tests (e.g. Berg Balance Scale (Berg, Wood-Dauphinee, Williams, & Gayton, 1989)) and posturography measures (e.g., sensory organization test (Cohen, Heaton, Congdon, & Jenkins, 1996)). These tests assess the ability to maintain standing balance and the quality of balance by measuring body sway. However, these tests do not determine the contribution and quality of the underlying mechanisms (Engelhart et al. 2014; Pasma et al., 2014). In addition, it is currently not

* Corresponding author.
E-mail address: d.engelhart@utwente.nl (D. Engelhart).

http://dx.doi.org/10.1016/j.arcontrol.2016.04.010
1367-5788/

possible to determine who has an increased risk of falling in the next year (Ganz, Bao, Shekelle, & Rubenstein, 2007; Laessoe, Hoeck, Simonsen, Sinkjaer, & Voigt, 2007; Visser, Carpenter, van der Kooij, & Bloem, 2008). Therefore, it is difficult to provide targeted interventions to decrease fall incidence. In other words, there is a clear (clinical) need to be able to (a) identify people with an increased fall risk, (b) evaluate targeted interventions, and (c) improve our overall understanding of the pathophysiology of balance-control impairments (Visser et al., 2008; Kingma et al., 2011; Sibley, Straus, Inness, Salbach, & Jaglal, 2013).

Estimation of the neuromuscular controller dynamics is difficult, as in a closed-loop feedback system (such as balance control) it is hard to disentangle cause and effect. That is, without externally applied disturbances, it is difficult to determine if, for example, changes in muscle activity result in changes in muscle force that will affect body sway, or that the opposite is true, i.e. changes in body sway are detected by sensors and transmitted to the nervous system that excites the muscle groups reflected in changes in the muscles' electromyography (EMG). Furthermore, standing balance is regulated around the ankles and hips, and multi-joint coordination must be achieved. Movements of one segment influence movements of the other segment (Horak & Nashner, 1986; Park, Horak, & Kuo, 2004), resulting in additional interactions.

System identification techniques in combination with specifically designed external disturbances provide a way to disentangle cause and effect in balance control and identify the dynamics of the neuromuscular controller. Therefore, our group (Van der Kooij, van Asseldonk, & van der Helm, 2005, 2007; Van Asseldonk et al., 2006; Boonstra, van Vugt, van der Kooij, & Bloem, 2014b; Engelhart et al., 2014; Pasma et al., 2014) and other groups (Johansson, Magnusson, a, & Karlberg, 2001; Peterka, 2002; Kim, Horak, Carlson-Kuhta, & Park, 2009, 2012; Jeka, Allison, & Kiemel, 2010; Mergner, 2010; Goodworth & Peterka, 2012) have developed and evaluated novel quantitative balance-control assessment methods based on system identification techniques to better understand the balance-control system, with the ultimate goal to improve clinical decision making. As the balance control system is dynamic (i.e., its response is described as a function of time), system identification techniques can be used to determine the underlying structures of the system by unraveling cause-and-effect relations in multi-joint coordination. The field of system identification is very broad, with many approaches and various techniques and methods. It is far from trivial to compare the methods reported in literature, as there are always differences in experimental design and the results are presented in different ways. If meaningful interpretation and comparisons are to be derived from balance-control experiments in different labs, there is a clear need for standardized protocols (Visser et al., 2008).

In this paper we compare different multivariable system identification techniques to estimate the neuromuscular controller dynamics with model simulations (as applied in literature), to evaluate the effects of various disturbance types and analysis methods. The advantage of model simulations is that all methods were validated based on one system from which all dynamics are known. We focused on methods that approached the human balance-control system as a double-inverted pendulum, pivoting at the ankles and hips in the anterior–posterior direction. This is contrary to many other methods that have approached the balance-control system as an inverted pendulum, with only an ankle joint. Our approach was chosen because recent studies have shown that differences between e.g. Parkinson's disease patients and the elderly (Boonstra, Schouten, van Vugt, Bloem, & van der Kooij, 2014a) and between the elderly and young (Accornero, Capozza, Rinalduzzi, & Manfredi, 1997; Hsu, Chou, & Woollacott, 2013) were the most pronounced in multi-segmental balance-control coordination.

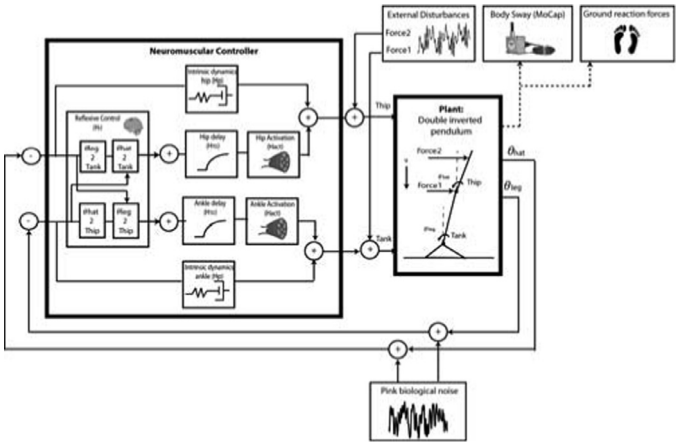

Fig. 1. Simple representation of the human balance control system. The human body is represented by a double-inverted pendulum, with a leg and a hat-arms-trunk (hat) segment. The neuromuscular controller generates corrective joint torques (T_{ank},T_{hip}) to regulate balance over time, by intrinsic dynamics (H_p) together with time-delayed (H_{TD}) reflexive activation (H_r, H_{act}) of muscles. For system identification purposes the body is disturbed by two external force disturbances at the hip and shoulder level, and body sway and ground reaction forces are measured.

Here, we give an overview of the applicability and (dis)advantages of various system identification techniques, which will aid toward the use of standardized measurement protocols to assess balance control with system identification techniques in a clinical setting.

2. Materials and methods

This section describes the general goal of system identification in human balance control, i.e. estimating the dynamics of the neuromuscular controller. By simulating a two-segmental balance-control model that contains the dynamics of the underlying physiology, various system identification techniques were presented, validated, and compared.

2.1. Modeling of human balance control

Fig. 1 shows a model of human balance control, in which the underlying physiology is described by various underlying mechanisms. When only considering anterior–posterior movement, the body dynamics can be regarded as a double-inverted pendulum, consisting of two segments; the lumped legs and the head-arms-trunk (hat) segment pivot around the ankle and hip joint respectively. Internal disturbances (biological noise in muscles, sensory organs, and the nervous system) and external disturbances (pushes and pulls on the human body and the pull of gravity) drive the system away from equilibrium. Maintaining standing balance is controlled by a feedback, i.e. a closed-loop system. The sensory systems (visual, vestibular, and proprioceptive) give information about the body position and velocity relative to the environment. These signals are processed and integrated by the CNS and fed back (with a neural transport delay) to the muscles. Corrective joint torques result from the activation of muscles (reflexive dynamics), together with intrinsic properties of the muscle-skeletal system (intrinsic dynamics). The entire neuromuscular controller describes how balance is regulated and is the system of interest in this study. This neuromuscular controller has separate feedback paths for the leg and hat segment and is therefore a multiple-input-multiple-output (MIMO) system.

2.2. System identification approach

2.2.1. External disturbances

Describing the dynamics of a (MIMO) system requires knowledge of the inputs and outputs of the system of interest. Here, the inputs of the neuromuscular controller are the leg and hat segment angles and the outputs are the corrective ankle and hip joint torques. In addition, an independent disturbance for each degree of freedom in the system is required (Pintelon & Schoukens, 2012). In this study we are interested in the contribution of the ankles and hip joints to balance control and therefore two disturbances must be applied. Applying only one disturbance can give erroneous results (Boonstra, Schouten, van der Helm, & van der Kooij, 2013), as responses remain intertwined. There exist various choices where to apply the two external disturbances (Fujisawa et al., 2005; Kiemel, Zhang, & Jeka, 2011; Boonstra et al., 2013), as long as they generate sufficient responses around each degree of freedom in the system. In this study, continuous push and pull disturbances were applied at the level of the hip and between the shoulder blades (Engelhart et al., 2015), see Fig. 1.

The external disturbances for system identification purposes are specifically designed as humans respond differently to fast or slow disturbances. The dynamic behavior of interest typically extents from 0.01 Hz to frequencies up until 4–5 Hz (van der Kooij & de Vlugt, 2007). Therefore, the external disturbances are broadband and excite the system in the region of interest. Furthermore, humans typically adjust to predictable disturbances and their responses may habituate. Therefore, the disturbances are unpredictable. Finally, the disturbances are submaximal. Therefore stance behavior is identified without making people step or fall, i.e. during feet-in-place responses. Various designs of such disturbance signals are described in the next paragraph.

2.2.2. Frequency response functions

All system identification techniques presented here assume linear and time-invariant (LTI) human behavior. This implies that the system does not change over the course of the experiment and that participants do not change strategy (e.g. switch from responding stiff to slack); i.e. the behavior does not change over time. Furthermore, when the participant is disturbed with a periodic signal, he/she will show periodic responses and the responses scale proportionally with the disturbances.

In such a LTI system, the human responses contain the same frequencies as the disturbances and the behavior of the system can be described in the frequency domain by a Frequency Response Function (FRF). The FRF consists of complex numbers, which can be expressed in a magnitude and phase. The entire dynamic behavior is generally displayed with a magnitude and phase plot that describes the differences in amplitude and timing respectively, between the inputs and outputs of a system as a function of frequency (f).

To be more specific, the FRF of the neuromuscular controller ($H_c(f)$) describes the dynamic relation, in the frequency domain, between the corrective joint torques (T_{ank}, T_{hip}) due to deviations in the segment angles (θ_{leg}, θ_{hat}) and consists of four terms:

$$\begin{bmatrix} T_{ank}(f) \\ T_{hip}(f) \end{bmatrix} = -\begin{bmatrix} H_{c,\theta_{leg}2T_{ank}}(f) & H_{c,\theta_{hat}2T_{ank}}(f) \\ H_{c,\theta_{leg}2T_{hip}}(f) & H_{c,\theta_{hat}2T_{hip}}(f) \end{bmatrix} \begin{bmatrix} \theta_{leg}(f) \\ \theta_{hat}(f) \end{bmatrix} \quad (1)$$

There are two direct terms covering the FRFs from leg angle to ankle torque ($H_{c,\theta_{leg}2T_{ank}}$) and from hat angle to hip torque ($H_{c,\theta_{hat}2T_{hip}}$). Furthermore, there are two indirect terms, which cover the FRFs from leg angle to hip torque ($H_{c,\theta_{leg}2T_{hip}}$) and from hat angle to ankle torque ($H_{c,\theta_{hat}2T_{ank}}$), which reflect the intersegmental coupling between the segments (Boonstra et al., 2013).

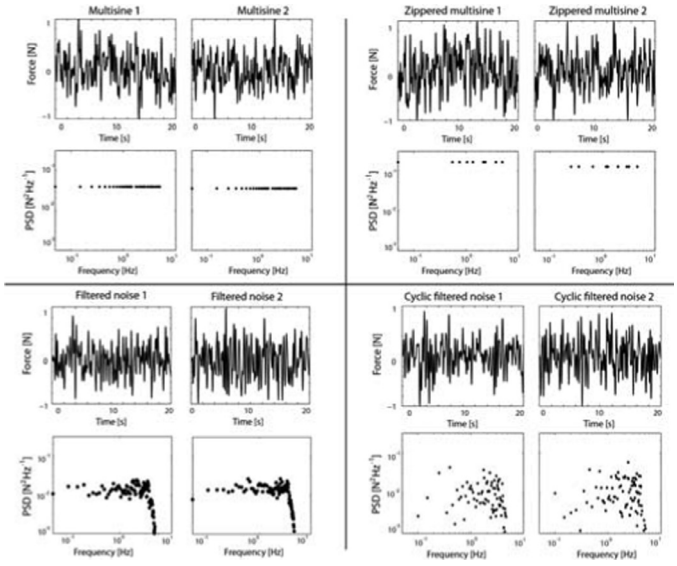

Fig. 2. Various disturbance signals for MIMO system identification. In the top rows the time series and in the bottom rows the power spectral densities (PSD). The filtered noise has a length of 180 s, but for comparison with the other signals, only 20 s are shown. The PSD of the filtered noise is smoothened by Welch averaging, with a 20 s Hanning window, with 50% overlap.

2.3. Disturbance signals

There are various design options for external disturbance signals. For system identification purposes, the disturbance signal should be sufficiently rich (power at many frequencies) and unpredictable to prevent a contribution of anticipation to the postural response. For proper application in the MIMO case, all the disturbance signals must be independent. Previous model simulations showed that disturbance signals with a flat power spectrum gave the best results, i.e. the lowest signal to noise ratio over the frequency range of interest (Boonstra et al., 2013).

Here, we focus on two main categories of disturbance signals, multisine and filtered noise. These two signals were commonly used in balance-control experiments where mechanical disturbances were applied (Engelhart et al., 2015; De Vlugt, Schouten, & van der Helm, 2006; Kiemel et al., 2011; Boonstra et al., 2014a). To make a fair comparison between the multisine and filtered noise signals, the frequency content of both signals was comparable. Furthermore, the root mean square (RMS) of the disturbances was the same to ensure equal energy was added to the system. Finally the amount of data was kept comparable between the signals (aiming for a measurement time of three minutes). Various designs of multisine and filtered noise signals were used in the simulations, as described below and shown in Fig. 2.

2.3.1. Multisine

Multisine signals consist of a sum of sinusoids; hence, the signals only contain power at specific frequencies. When each harmonic fits exactly an integer number of times in the multisine signal, leakage in the frequency domain analysis can be prevented. This is assured by only including harmonics with frequencies equal to an integer multiple of the frequency resolution. As the frequency resolution is the inverse of the period of the multisine signal, the lowest frequency of interest is therefore directly related to the measurement time. To apply multisine signals for MIMO application, two multisine signals can have equal frequency content, but in this case the signals are not independent. To create the independent signals for each input, the experiment is repeated with

two different combinations of the multisine (Pintelon & Schoukens, 2012).

In this study, a random phase multisine signal with a period of 20 s was generated, in which a total of 27 frequencies were logarithmically spaced in a frequency band of 0.05 and 5 Hz. Here, the multisine signals were repeated five times, resulting in a trial length of 100 s. In the first trial, both inputs were excited with the same multisine, while in the second trial the sign of the second input was changed. This resulted in a total measurement time of 200 s, approximately three minutes.

2.3.1.1. Zippered multisine. Another possibility is to design two multisine signals with one excited frequency only appearing in one signal. The input signals are chosen such that each disturbance contains a number of excited frequencies at an interleaved frequency grid, termed a zippered multisine (Pintelon & Schoukens, 2012). The advantage compared to a multisine disturbance is that a zippered multisine fully characterizes a MIMO system from a single experiment. To characterize a closed-loop system with zippered multisine requires interpolation to the full frequency grid, which is described in the data analysis section.

In this study, a zippered multisine disturbance was generated in which a total of 27 frequencies (equal to the multisine signal) were logarithmically spaced in a band between 0.05 and 5 Hz. From each set of three odd harmonics, one was randomly assigned to the first disturbance, one was randomly assigned to the second disturbance, and the third one was not excited. The zippered multisine had a period of 20 s and was repeated nine times, leading to a measurement time of 180 s.

An additional advantage of using multisine is that the assumption of linearity can be tested. As only random odd harmonics are excited, even nonlinearities become visible when there is power at the even frequencies, while the odd non-excited frequencies can be used to detect and quantify the power level of the odd nonlinearities. For model simulations, the outcomes are trivial (as the equations of motion are linearized), but for experiments one can obtain additional information about the reliability of the FRF.

2.3.2. Filtered noise

White noise consists of all frequencies with equal power and is a representation of a purely stochastic process. As each value is uncorrelated to the other values, two white noise disturbances are naturally independent.

In this study, two filtered noise signals of 180 s were generated comparable to (Kiemel et al., 2011). Two white noise signals were passed through a first-order high-pass filter with a cut-off frequency of 0.05 Hz and an eight-order Butterworth low-pass filter with a cut-off frequency of 5 Hz. The power spectral density was computed using Welch's method with a 20-s (comparable to the length of the multisine signal) Hanning window and 50% overlap. This created a flat power spectrum comparable to the multisine signals. The filtered noise signals had a length of 180 s.

2.3.2.1. Cyclic filtered noise. It is also possible to generate cyclic filtered noise as input signals to allow for averaging in time over the sequences to reduce noise. Two filtered noises of 20 s were generated, similar as described above. The signals were repeated nine times, leading to a measurement time of 180 s.

2.4. Model simulations

Model simulations were performed on the two-segment human balance control model, (Matlab Simulink (The MathWorks, Natick, MA)) with a leg and hat segment, and a neuromuscular controller as shown in Fig. 1. The model was based on a previous study (Boonstra et al., 2013) and is extensively described in the Appendix. Two external force disturbances with a peak-to-peak amplitude of 80 N were applied at the level of the hip and the shoulders in five simulated trials of 180 s, in which the disturbance signals varied:

(1a) Two multisine disturbances with equal frequency content.
(1b) Disturbance signals as in trial 1, in which the sign of one perturbation is reversed
(2) Zippered multisine disturbance
(3) Filtered noise disturbance
(4) Cyclic filtered noise disturbance

These simulations rendered the time series of the segment angles and joint torques at a sample frequency of 1 kHz, which were processed offline in Matlab (The MathWorks, Natick, MA). To make the model simulations realistic and to compare them to experimental measurements, additional noise was included. Biological noise originates from inaccuracies in the sensory systems and the motor system. This biological noise is believed to be of pink origin, meaning the power spectral density (power per frequency (f)) is inversely proportional to the frequency ($\frac{1}{f^a}$). In our simulations, pink noise with $a = 1.2$, was added to the system, such that during quiet stance, the sway angle (remnant sway) was comparable to data of standing balance (van der Kooij & Peterka, 2011). Furthermore, measuring human responses includes measurement noise due to the equipment. This was modeled as a zero mean white noise source (variance of $1 * 10^{-6}$) added to the states (segment angles and angular velocities), and to the ankle and hip joint torques.

2.5. Data analysis

Based on the applied disturbances and the rendered segment angles and joint torques (with model simulations), various system identification techniques were used to analyze the simulated data. The aim was to estimate the dynamic behavior of the neuromuscular controller, which ideally compares exactly to the theoretical model as described in the Appendix. The system identification methods can be divided in two main categories: non-parametric system identification techniques and parametric system identification techniques (Table 1). Please note that the use of methods and disturbance signals is intertwined. Table 1 shows if the system identification method performs well in combination with a specific disturbance signal. Also note that although the model is simulated in continuous time, the system identification techniques are based on sampled data and therefore the analysis is time discrete. The performance of the methods was evaluated based on validation criteria in the time and frequency domain, as described at the end of this section.

2.5.1. Non-parametric system identification techniques

Non-parametric system identification techniques express the system behavior in the frequency domain by means of an FRF, without *a priori* knowledge of the system. To extract the neuromuscular controller properties from the closed loop system, the Joint-Input-Output-Method is applied (Van der Kooij et al., 2005). The closed-loop is opened by relating the signals in the loop to the external disturbances. The FRF of the neuromuscular controller ($H_c(f)$) is described by:

$$H_c(f) = -S_{dT}(f)(S_{d\theta}(f))^{-1} \quad (2)$$

In which S_{dT} and $S_{d\theta}$ are the cross-spectral density (CSD) matrices between the external disturbances ($d(f)$) to the segment angles ($\theta(f)$) and joint torques ($T(f)$). The methods as described below, differ in the applied external disturbance signal and thereby the method of calculating the CSD matrices.

Table 1
Various system identification techniques with corresponding disturbance signals. Some methods perform well with a specific disturbance signal (indicated by a √), as some methods cannot be applied with a specific disturbance signal (indicated by a x).

	Multisine	Filtered noise
Non-parametric system identification techniques		
(1) Two experiments (2EXP)	√	X
(2) Interpolation (INT)	√	X
(3) Partial coherence (PC)	X	√
Parametric system identification techniques		
(4) Multiple least square (MLSQ)	√	√
(5) Optimization (OPTIM)	√	√
(6) Autoregressive–moving-average model with exogenous inputs (ARMAX)	√	√
(7) Predictor-based subspace identification (PBSID)	X	√

2.5.1.1. Method 1: two experiments (2EXP). This method is based on previous studies (Pintelon & Schoukens, 2012; Boonstra et al., 2013, 2014b), where the external disturbance signals are multisine disturbances. The disturbance signals were applied in two experiments, in which the sign of the second disturbance is reversed in the second experiment, compared to the first experiment.

The time series of the disturbance signals, segment angles, and joint torques ($d(t)$, $\theta(t), T(t)$) were segmented in 10 repetitive cycles of the disturbance signal (two experiments with five cycles). The segmented time series were averaged to reduce noise, prior to analysis.

Subsequently, data was transformed to the frequency domain by a fast Fourier transformation ($d(f)$, $\theta(f), T(f)$) and the CSD matrices from the external disturbances to the segment angles ($S_{d\theta}(f)$) and joint torques ($S_{dT}(f)$) were calculated. The FRF of the neuromuscular controller ($H_c(f)$) resulted from Eq. (2).

2.5.1.2. Method 2: interpolation (INT). This method is based on a previous studies (Pintelon & Schoukens, 2012; Engelhart et al., 2014), where the external disturbance signals are zippered multisines. The time series of the disturbance signals, segment angles, and joint torques ($d(t)$, $\theta(t), T(t)$) were segmented in nine repetitive cycles of the disturbance signal. Subsequently, data was transformed to the frequency domain by a fast Fourier transformation. The Fourier coefficients of the disturbances, angles, and torques ($d(f)$, $\theta(f), T(f)$) were averaged in the frequency domain to reduce noise, prior to analysis. Calculating the CSD matrices ($S_{d\theta}(f)$), $S_{dT}(f)$), requires that the matrix components are known at all excited frequencies, which is untrue for the zippered multisine, as both input signals contain different frequencies. Therefore, the complex numbers of the cross spectral densities were interpolated in terms of magnitude and phase.

Consequently, all matrix components for the full range of excited frequencies in the zippered multisine were obtained, and it was possible to identify the neuromuscular controller ($H_c(f)$) using Eq. (2).

2.5.1.3. Method 3: partial coherence (PC). This method is based on previous studies (Perreault, Kirsch, & Acosta, 1999; De Vlugt, Schouten, & van der Helm, 2003, 2006; Kiemel et al., 2011), where the external disturbance signals are filtered noise. The time series of the disturbance signals, segment angles, and joint torques ($d(t)$, $\theta(t), T(t)$) were transformed to the frequency domain by a fast Fourier transformation ($d(f)$, $\theta(f), T(f)$). Because both filtered noise disturbances contain equal frequency content (matrix division is possible) and they are naturally uncorrelated, elicited responses can be related to either disturbance. The CSD matrices ($S_{d\theta}(f)$), $S_{dT}(f)$) were computed using Welch's method with 20 s Hanning windows and 50% overlap. Consequently, the FRF of the neuromuscular controller ($H_c(f)$) was calculated with Eq. (2).

2.5.2. Parametric system identification techniques

Parametric system identification techniques express the behavior of a system in a model with a limited number of parameters. The behavior of a system is described by a mathematical function, relating signals with respect to time. Often *a priori* assumptions about the order of the system and the model structure are required. Methods 4 and 5 as described below only estimate the dynamic behavior of the system, while methods 6 and 7 also give an estimation of the noise in the system.

2.5.2.1. Method 4: multiple least squares (MLSQ). Early studies (Barin, 1989; Winter, Patla, Rietdyk, & Ishac, 2001) used a multiple least squares algorithm to compute a feedback gain matrix (K), which describes the relation between the states ($x(t)$) of the human balance control system and the corrective joint torques ($T(t)$) in the time domain.

$$T(t) = -Kx(t)$$

$$\begin{bmatrix} T_{ank}(t) \\ T_{hip}(t) \end{bmatrix} = -\begin{bmatrix} k_{11} & k_{12} & d_{11} & d_{12} \\ k_{21} & k_{22} & d_{21} & d_{22} \end{bmatrix} \begin{bmatrix} \theta_{leg}(t) \\ \theta_{hat}(t) \\ \dot{\theta}_{leg}(t) \\ \dot{\theta}_{hat}(t) \end{bmatrix} \tag{3}$$

The feedback gain matrix K was found by a least square estimation:

$$K = -\mathbb{T}\mathbb{X}^T\left(\mathbb{X}\mathbb{X}^T\right)^{-1} \tag{4}$$

where $\mathbb{X}$ and $\mathbb{T}$ are matrices in which each row corresponds to a state or a corrective joint torque, respectively, and each column corresponds to a time sample. The feedback gain matrix K was used to determine the FRF of the neuromuscular controller; $H_c(f)$ is quantified as a combination of stiffness (k) and damping (d) values

$$\begin{bmatrix} T_{ank}(f) \\ T_{hip}(f) \end{bmatrix} = -H_c \begin{bmatrix} \theta_{leg}(f) \\ \theta_{hat}(f) \end{bmatrix}$$

$$H_c = \begin{bmatrix} k_{11} + d_{11} * j2\pi f & k_{12} + d_{12} * j2\pi f \\ k_{21} + d_{21} * j2\pi f & k_{22} + d_{22} * j2\pi f \end{bmatrix} \tag{5}$$

In which $j2\pi f$ expresses the Laplace transform, i.e. the derivative in the frequency domain.

In this study, we applied both multisine as well as filtered noise disturbances to excite the system. The time series of the states, i.e. segment angles and angular velocities ($\theta(t), \dot{\theta}(t)$) and the joint torques ($T(t)$) were segmented in nine repetitive cycles of the disturbance signal. The segmented time series were averaged to reduce noise, prior to analysis.

2.5.2.2. Method 5: optimization (OPTIM). In a more recent study (Park et al., 2004), an optimization algorithm was used for estimating the feedback gain matrix K. Eq. (6) shows that different from the multiple least squares method, the states ($x(t)$, segment angles, and angular velocities) were simulated (in continuous time) based on knowledge of the biomechanics of the human (assumed to be a double-inverted pendulum (2IP) and captured in an A_{2IP} and B_{2IP} matrix), the estimated K matrix, and the applied external disturbance signals (matrix W). Consequently, the corrective joint torques were derived from the states and the estimated K matrix. The objective (cost function) of the optimization process was to find the optimal feedback gain matrix K, based on the lowest sum-squared error between the estimated and true states and estimated and true torques.

$$\begin{aligned}\dot{x}(t) &= A_{2IP}x(t) + B_{2IP}u(t) + W\\ \text{With } u(t) &= T(t) = -Kx(t)\\ \dot{x}(t) &= (A_{2IP} - B_{2IP}K)x(t) + W\end{aligned} \tag{6}$$

In this study, we applied both multisine as well as filtered noise disturbances to excite the system. The time series of the states, i.e. segment angles and angular velocities ($\theta(t), \dot{\theta}(t)$) and joint torques ($T$(t)) were segmented in nine repetitive cycles of the disturbance signal. The segmented time series were averaged to reduce noise, prior to analysis. The optimization algorithm was repeated 10 times using initial guesses (random values within bounds) for K, to check for local minima in the optimization. If a minimum was found repeatedly, a global minimum was assumed and the corresponding K matrix was implemented in Eq. (5) to estimate the neuromuscular controller $H_c(f)$.

2.5.2.3. Method 6: autoregressive-moving-average model with exogenous inputs (ARMAX). Another commonly used group of parametric system identification techniques are prediction error methods (PEM). In PEM methods, the output of the system as obtained from measurements is compared to the output as predicted by the model. The difference between the two is termed the prediction error and indicates how well the model represents the data. The model includes parameters that describe the system behavior, and additionally includes parameters that describe the noise in the system. Various model structures have a different parameterization of the system and noise model (Ljung, 1999). In a previous study (Fujisawa et al., 2005), an ARMAX model was used to model balance control, in which output $y(t)$ is related to the input $u(t)$ and noise $e(t)$:

$$A\left(z^{-1}\right)y(t) = B\left(z^{-1}\right)u(t) + C\left(z^{-1}\right)e(t) \tag{7}$$

In which z^{-1} is the shift operator to describe past discrete time samples. The A and B polynomial matrices describe the estimation of the system, how u (the segment angles) are related to y (the joint torques), depending on a number of parameters (order of the system). Increasing the number of parameters will improve estimation, as the estimated structure better compares to the data. However, a large number of parameters increases the computational burden and possibly does not further reduce the prediction error. A trade-off between the lowest number of parameters and a low prediction error must be made, which is often expressed in Akaike's Information Criterion (Ljung, 1999).

The validity of the estimation (consistency) can be determined by residuals analysis. The residuals are the remaining errors between the real model and the identified model. When the autocorrelation of the residuals represents white noise, this is an indication that the noise dynamics are fully captured. The cross-correlation between the inputs and residuals indicates whether or not the system model is captured. An advantage of these residual tests is that the accuracy of a model is determined by only using the available data. Residual outcomes directly explain whether the identified model can represent the system dynamics within specified confidence levels.

In this study, we applied both multisine and filtered noise disturbances. To improve consistent outcomes of an ARMAX model (which favors high frequencies in the optimization process), data was resampled to 10 Hz. As we are dealing with a MIMO and closed-loop system, first a consistent ARMAX model was estimated for the relation between the disturbances and torques, resulting in $H_{dT}(f)$. Subsequently a consistent ARMAX model was estimated for the relation between the disturbances and angles, resulting in $H_{d\theta}(f)$. The obtained models are divided resulting in an estimation of the neuromuscular controller properties, comparable to Eq. (2).

2.5.2.4. Method 7: predictor-based subspace identification (PBSID). In the predictor-based subspace identification method (Ljung, 1999) (van Wingerden, 2008), the LTI system is considered in state space:

$$\begin{aligned}(t + t_s) &= A_{ss}x(t) + B_{ss}u(t) + K_{ss}e(t)\\ y(t) &= C_{ss}x(t) + D_{ss}u(t) + e(t)\end{aligned} \tag{8}$$

with a sample time t_s and where $x(t), u(t), y(t)$ are the state, input and output vectors as functions of time, respectively. The vector $e(t)$ denotes the zero mean white noise sources. The state space matrices $A_{ss}, B_{ss}, C_{ss}, D_{ss}, K_{ss}$ are the system, input, output, direct feed-through, and observer matrices. The goal of the PBSID method is: Given the input sequence $u(t)$ (the two disturbances) and output sequence $y(t)$ (ankle and hip angles and corrective torques), find all the state space matrices of the system up to a global similarity transformation. If the states $x(t)$ were known, the solution would be straightforward: compute C and D with linear regression, reconstruct the noise $e(t)$, and compute A_{ss}, B_{ss}, K_{ss} with linear regression. However, the problem is to find the states.

An essential step in subspace identification is to reconstruct the (extended) observability matrix (Γ) from input and output data (Verhaegen, 2007).

$$\Gamma^{n} = \begin{bmatrix} C_{ss} \\ C_{ss}A_{ss} \\ \vdots \\ C_{ss}A_{ss}^{\,n-1} \end{bmatrix} \tag{9}$$

A system is said to be observable if the states of the system can be inferred through linear combinations of the system outputs. This means that from knowledge of the system's outputs, it is possible to determine the behavior of the entire system. The system is observable when the rank of this matrix equals the amount of states (n), which gives the order of the system. A singular value decomposition can be used for order determination. Once the rank and the observability matrix are known, the A_{ss} and C_{ss} matrix can be determined as matrix C_{ss} equals the first rows (dependent on the number of outputs) of the observability matrix and A_{ss} can be determined from the rest. Additionally, the states and the noise contributions can be estimated, together with the B_{ss} and D_{ss} matrices with linear regression.

Due to the state-space description of the system, the method can implicitly handle MIMO systems, and common structures between disturbances, segment angles, and corrective torques are incorporated. Also as an advantage compared to PEM methods, determination of the system order was incorporated in the algorithm and no *a priori* assumptions about the model structure were needed. The estimates for both $H_{dT}(f)$ and $H_{d\theta}(f)$ were therefore found in just one identification step, converting the state space model to a frequency response, with the disturbances expressed as two inputs and the segment angles and corrective joint torques

as four outputs. The frequency response was only calculated for the excited frequencies in the disturbance signals.

$$\begin{bmatrix} \theta_{leg}(f) \\ \theta_{hat}(f) \\ T_{ank}(f) \\ T_{hip}(f) \end{bmatrix} = \begin{bmatrix} H_{d\theta}(f) \\ H_{dT}(f) \end{bmatrix} \begin{bmatrix} d_{pelvis}(f) \\ d_{shoulder}(f) \end{bmatrix} \quad (10)$$

Based on the transfer function matrices for both H_{dT} and $H_{d\theta}$, the neuromuscular controller can be obtained using Eq. (2). In this study, we applied both multisine as well as cyclic filtered noise disturbances.

2.6. Validation criteria

To quantify how well the obtained neuromuscular controller descriptions represent the true system, we have used validation criteria for both the time and frequency domain.

2.6.1. Goodness of fit (GOF)

Based on simulated data, the theoretical FRF of the neuromuscular controller can be compared with the identified FRF of the system identification method. This goodness of fit (GOF) is calculated as the logarithmic absolute and squared difference between the estimated neuromuscular controller FRF ($\widehat{H_c}(f)$) and the theoretical FRF ($H_c(f)$), averaged over the amount of frequencies in the disturbance signal.

$$\text{GOF} = \frac{1}{n_f} \sum_{f=0.05}^{5} \left| \ln\left(H_c(f)\right) - \ln\left(\hat{H}_c(f)\right) \right|^2 \quad (11)$$

The number of excited frequencies differs for each disturbance signal (i.e., multisine $n_f = 27$, zippered multisine $n_f = 18$, filtered noise $n_f = 100$). A low GOF indicates a good fit.

2.6.2. Variance accounted for (VAF)

Once a parametric estimate of the system is available, the behavior of the neuromuscular controller can be used to predict the outputs of the system by simulating the model using the corresponding inputs. The percentage of Variance Accounted For (VAF) represents the quality of the identified model by comparing the measured output ($y(t)$) with the simulated output ($\hat{y}(t)$) in the time domain. The VAF of two equal signals will be 100%. If they differ, the VAF will be lower (Verhaegen, 2007).

$$VAF\left(y(t), \hat{y}(t)\right) = \left(1 - \frac{var\ \left(y(t) - \hat{y}(t)\right)}{var\ \left(y(t)\right)}\right) * \ 100\% \quad (12)$$

In case of a non-parametric estimate, the Fourier components of the open loop transfer functions $S_{dT}(f)$ and $S_{d\theta}(f)$ were multiplied with the Fourier components of the disturbances. The inverse Fourier transform of this product results in the outputs of the system, the angles or torques respectively. Comparing these "simulated" outputs to the measured outputs gives the VAF. In case of cyclic disturbances (multisine and zippered multisine signals), this measure describes how each cycle deviates from the mean over cycles, which is comparable to a noise-to-signal ratio.

2.6.3. Measurement time

In balance-control experiments, it is advantageous to have short experimental measurement times. Especially in impaired standing balance, subjects become easily fatigued, which induces time variant behavior. Therefore the amount of measurement time, i.e. amount of data needed for identification, is also a validation factor and was studied by using various simulation times.

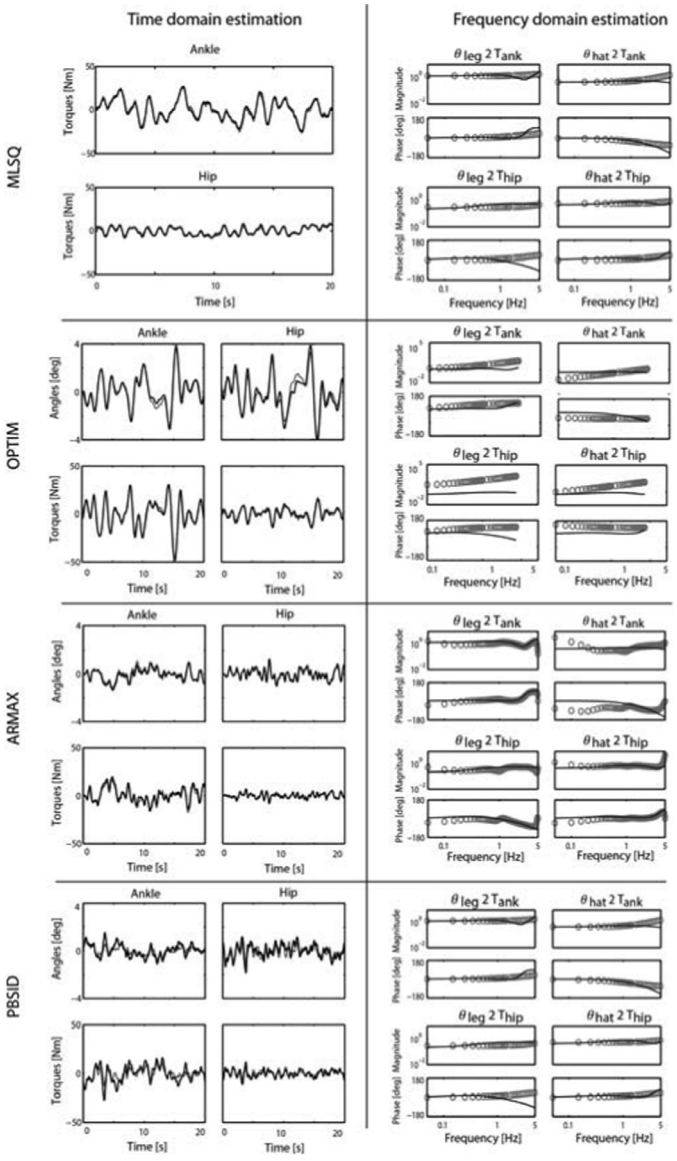

Fig. 3. Parametric system identification of the neuromuscular controller in time domain (left) and frequency domain (right) based on simulated data. For the MLSQ and OPTIM, multisine signals were used, and for the ARMAX and PBSID method, filtered noise signals were used. For the time domain estimation, the simulated time series are shown in black, and the estimated time series are shown in grey. For the frequency domain estimation, the theoretical FRF of the model is shown by the black solid line and the estimated FRF on the excited frequencies is shown by the grey circles.

3. Results

3.1. Non-parametric system identification techniques

Non-parametric spectral-system identification techniques were especially designed for the estimation of system dynamics in the frequency domain. Fig. 3 shows that with non-parametric system-identification techniques, the neuromuscular controller dynamics were estimated well. Hence, for all methods and various external disturbance signals, the estimated dynamics were close to the theoretical FRF.

Table 2 gives an overview of the validation criteria for the various methods. In the frequency domain, the fits were all good, as can be seen from the relatively low GOF values. The GOF value for the 2EXP method was lowest, followed by the INT method, and the

Table 2
Validation of the system identification techniques, based on model simulations.

	Multisine							
	GOF				VAF (%)			
Method	$\theta_{leg}2T_{ank}$	$\theta_{hat}2T_{ank}$	$\theta_{leg}2T_{hip}$	$\theta_{hat}2T_{hip}$	θ_{leg}	θ_{hat}	T_{ank}	T_{hip}
2EXP	0.01	0.03	0.01	0.00	97	97	98	99
INT	0.01	0.08	0.01	0.01	98	99	99	99
PC	–	–	–	–	–	–	–	–
MLSQ	0.35	0.58	1.75	0.13	–	-	98	92
OPTIM	18.39	8.36	43.45	21.32	94	90	96	88
ARMAX	0.75	2.53	1.78	0.88	94	98	93	85
PBSID	0.33	0.30	1.35	0.08	0	0	0	0
	Filtered noise							
	GOF				VAF (%)			
Method	$\theta_{leg}2T_{ank}$	$\theta_{hat}2T_{ank}$	$\theta_{leg}2T_{hip}$	$\theta_{hat}2T_{hip}$	θ_{leg}	θ_{hat}	T_{ank}	T_{hip}
2EXP	–	–	–	–	–	–	–	–
INT	–	–	–	–	–	–	–	–
PC	0.02	0.49	0.22	0.01	83	90	89	93
MLSQ	0.54	0.70	1.57	0.18	–	–	98	93
OPTIM	29.28	16.52	56.60	34.47	89	83	71	60
ARMAX	0.56	0.40	0.52	0.38	91	96	93	91
PBSID	0.55	0.39	0.52	0.38	67	63	66	71

PC method had the highest GOF value. In the time domain, the VAF values were high for all methods. The 2EXP and INT method had a slightly higher VAF than the PC method. Please note however, that in case of T_{hip}, the RMS of the error in case of a VAF of 93% (PC method) more than doubles compared to a VAF of 99% (2EXP and INT method).

The amount of measurement time was kept similar between the non-parametric system identification techniques. Exciting the system with multisine signals had the advantage that in case this periodic signal was repeated during the experiment (which we did), averaging over the successive repetitions decreased the noise. This potentially reduced the amount of data that was needed to obtain a reliable non-parametric estimate of the neuromuscular controller. Increasing the amount of repetitive cycles of a multisine signal decreased the GOF, i.e. the FRF resembled the theoretical one better. Averaging over more cyclic filtered noise repetitions decreased noise in the system and estimated the FRF better; however the effect was less than for the multisine. Segmenting a filtered noise signal in more segments and applying smoothing using a Hanning window to compute the CSD also reduced noise and gave a better estimation. However, the drawback was that it also influenced the lowest frequency, which you could identify.

3.2. Parametric system identification techniques

Parametric-system identification techniques were especially designed for the estimation of system dynamics in the time domain. Fig. 4 shows the simulated and identified time series for all the parametric methods. The identified time series were comparable to the simulated time series, indicating a good fit. Table 2 shows that in general, the VAF values for the multisine disturbances were slightly higher compared to the application of the filtered noise disturbances. The VAF values were above 85% in case of multisine disturbances, indicating a good estimation of the system dynamics in the time domain. Except for the PBSID method, which had a very poor fit using multisines as external disturbance signals. A better fit was obtained with filtered noise, however the VAF was below 75%, indicating the RMS value of the error is half the RMS value of the disturbance signal.

However, when the estimated model was evaluated in the frequency domain, the methods performed less, as can be seen from the relatively high GOF values. The estimated dynamics deviated from the theoretical FRF of the neuromuscular controller.

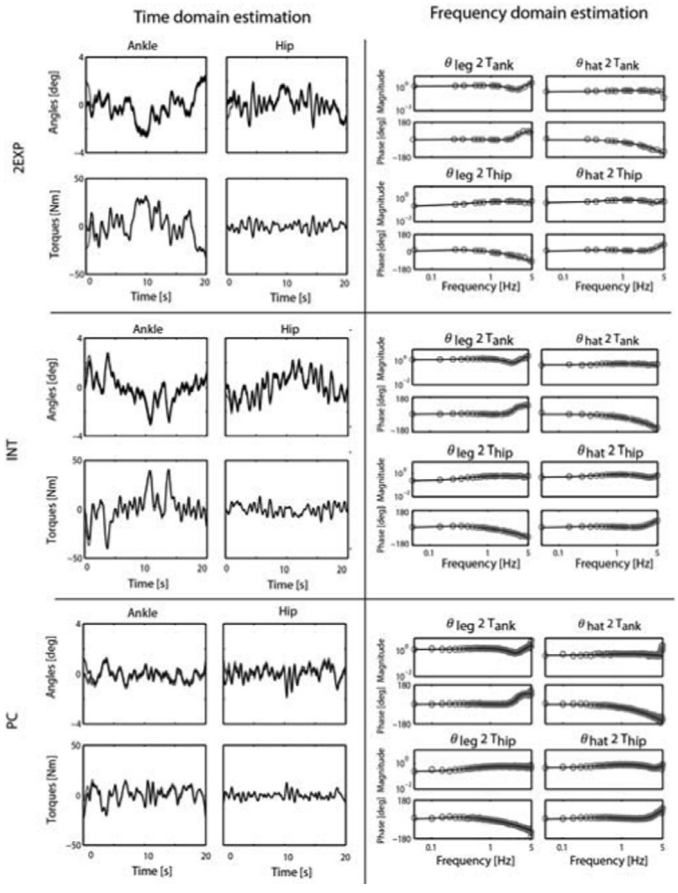

Fig. 4. Non-parametric system identification of the neuromuscular controller in time domain (left) and frequency domain (right) based on simulated data. For the time domain estimation, the model simulated time series (ankle and hip angles and torques) are shown in black, and the estimated time series based on the system identification methods are shown in grey. Comparing these gives an indication of the goodness of fit. For the frequency domain estimation, the FRF of the simulated model is shown by the black solid line and the estimated FRF (with system identification methods) on the excited frequencies is shown by the grey circles.

Fig. 4 clearly shows the mismatch between the theoretical and estimated FRF, which was largest for the OPTIM method.

Comparable to the non-parametric system identification techniques, the amount of measurement time was kept similar between the parametric system identification techniques. Again, applying a periodic signal (such as a multisine) improved the estimation of the mean responses as noise was averaged out.

The feedback gains or estimated model were therefore a more reliable representation of the system. However, in parametric models, the estimated model depended much more on the model structure and the order than on the amount of available data.

4. Discussion

Based on model simulations, we evaluated various MIMO closed-loop system identification techniques in combination with external disturbance signals. Results indicated that non-parametric techniques with (zippered) multisine disturbances gave the most accurate estimation in the time (highest variance accounted for) and frequency (lowest goodness of fit) domain of the neuromuscular controller mechanisms. The use of zippered multisines had the advantage that only one experiment had to be performed, in contrast with the full multisine disturbance, which required two experiments. Parametric system identification techniques did not estimate all the underlying neuromuscular controller dynamics. Although the time series were estimated reliably, the dynamics in the frequency domain were not fully captured.

4.1. Evaluation of system identification techniques

We evaluated seven methods to estimate the dynamics of the MIMO neuromuscular controller. The methods were divided in two main approaches: (1) non-parametric system identification techniques, and (2) parametric system identification techniques. We evaluated all methods with simulated data using three quantitative evaluation criteria: variance accounted for (VAF), goodness of fit (GOF), and measurement time.

4.1.1. Non-parametric system identification techniques estimated the dynamics of the neuromuscular controller well for various disturbance signals

Non-parametric spectral techniques can be applied in combination with various disturbance signals, as long as they contained multiple frequencies in the range of interest and the signals were sufficiently exciting the system. A drawback of the 2EXP method is that two experiments are required to estimate the neuromuscular controller dynamics. This inherently assumes that the system dynamics remain equal over the two experiments, which is not always the case (e.g. humans get fatigued, which can change their behavior or strategy). A drawback of the INT method is the interpolation of the frequency grid, which possibly induces an error in the FRF, in case the excited frequencies are further apart. The choice of disturbance signal depends on the application, and all signals have advantages and disadvantages. We elaborated on this further in the section about disturbance signal choice.

4.1.2. Parametric system identification techniques were difficult to apply in human balance control due to the assumed model structure and biological noise in the system

Parametric system identification techniques estimate a structure through excited frequencies; our results showed that this worked best when all frequencies in the range of interest were excited, i.e. filtered noise signals. Nevertheless, the methods performed well while using multisine signals with many excited frequencies. Four parametric system identification techniques were used to analyze the data, of which two were based on estimation of a feedback gain matrix using multiple least squares and optimization techniques. Furthermore, we have evaluated a Prediction Error Method (ARMAX) and a Predictor-Based Subspace Identification (PBSID) method.

4.1.2.1. Multiple least squares and optimization techniques. The MLSQ and OPTIM techniques have been applied previously to estimate the general control mechanisms in balance control (Barin, 1989; Winter et al., 2001). These studies showed that the postural feedback gains scaled with the disturbance magnitude and type (Park et al., 2004), and changed with age (Speers, Kuo, & Horak, 2002). One should note that the system identification algorithm of the MSLQ and OPTIM method does not only include information about the segment angles, but also uses the angular velocities. Therefore these methods have more information about the system than the other methods, which may explain the good fit in the time domain. In our study, model simulations showed that the MLSQ and OPTIM methods yielded erroneous results in estimating the dynamics of the neuromuscular controller. This effect was expressed the most in the frequency response functions at the higher frequencies, whereas the time domain fits were quite good. This misfitting in the frequency domain was probably due to the fact that the feedback gain matrix assumed that the underlying mechanisms of the neuromuscular controller consisted of springs and dampers. This is, however a simplification; the model neuromuscular controller also included time delays and muscle-activation dynamics, which were not captured in these estimation methods. Furthermore, the least square estimation might result in biased outcomes, as the closed loop system is not taken into account; i.e. the signals might be correlated due to feedback.

4.1.2.2. Prediction error methods. A disadvantage of parametric methods in general is that a model structure was assumed and a specific order was estimated and both the estimation of the order and the model structure can be wrong. For example, an ARMAX model has a dependent structure for the noise and system model (Ljung, 1999). If the estimation of the noise model is incorrect, this affects the estimation of the system model. For example, the biological pink noise in our system does not match the assumed linear noise model. Future research might elaborate on the use of other PEM models structures, such as Box–Jenkins models, where the noise and system model are independent. Furthermore, the division of two parametric estimates (which both contain errors) can give inaccurate results, as the errors are present in the closed-loop estimation. These errors might be due to inaccurate estimation of time delays in the system. An ARMAX structure assumes a time delay in its model structure. The neuromuscular controller as presented in our study, consists of feedback paths with a mixture of time delays (reflexive feedback) and no delays (intrinsic feedback); this cannot be fully captured (only approximated) by the model structure of the parametric estimation. Therefore, it is important to check the residuals of the estimation to verify the correctness of the system and noise model.

ARMAX models have been applied in a previous study (Fujisawa et al., 2005), identifying the MIMO neuromuscular postural control mechanisms. However, the excited frequencies only extended until 0.83 Hz. From our model simulations it was seen that the dynamics of balance control extended to approximately 4 Hz and therefore in this study, we used a broadband disturbance signal.

4.1.2.3. Predictor based subspace identification . The advantage of the PBSID method is that the MIMO neuromuscular controller was estimated in one identification step, without dividing two parametric estimates, reducing the errors in the estimation. A disadvantage of subspace methods is that they were designed to estimate the model structure for the case that all noise sources acting

on the system are white. However, biological noise (internal disturbances from the sensory and the motor system) is thought to be of pink noise origin (van der Kooij & Peterka, 2011), which has the highest power in the low frequencies. As we are dealing with this biological noise in the feedback mechanism, obtaining a correct estimation can be a challenge. Nevertheless, subspace identification might be a field of further research, as it allows for studying the variation over time (see the section about time invariance).

4.1.3. Multisine signals are the optimal choice of disturbance signals

Non-parametric system identification techniques do not have the drawbacks that were mentioned in the previous paragraph. The advantage of non-parametric system identification techniques is that the system dynamics can be estimated without a priori knowledge of the system; i.e. these methods do not suffer from inaccurate model structures. Furthermore, the noise in the system is not identified and therefore the FRFs are not influenced by the assumption of pink biological noise. We used four different disturbance signals (multisine, zippered multisine, filtered noise, and cyclic filtered noise) and evaluated their effectiveness. Below we discuss why multisines are the optimal choice of disturbance signal.

First, compared to filtered noise signals, multisine disturbances have no leakage errors as each harmonic fits exactly an integer number of times in the multisine signal (Pintelon & Schoukens, 2012). In case of leakage, power has leaked out to other frequency bins, which affects the FRF estimate. Secondly, averaging over the repetitive cycles of the disturbance signal reduces noise. Therefore the noise-to-signal ratio (NSR) of the multisine signal is lower than the NSR of the filtered noise disturbances. Finally, exciting fewer frequencies improves NSR further, as there is only (and therefore increased) power at the frequencies of interest. Hence, multisine disturbances have higher NSR compared to filtered noise, and this effect is even stronger when using a zippered multisine.

Furthermore, there is a difference in frequency resolution between the signals. If you are dividing the frequencies over multiple disturbances, thereby creating a zippered multisine, the frequency resolution drops. Therefore, a drawback of multisine disturbances, and even more in zippered multisine disturbances, is that only specific frequencies are excited, making it insensitive to what happens between those frequencies; e.g., very narrow resonance peaks can be missed.

An advantage of the zippered multisine is that only one experimental trial was needed, which reduced the time to overcome transients by two at the beginning of the measurement trial, compared to the multisine method.

In sum, the choice of the “optimal” multisine signal is a trade-off between frequency resolution (design choices in the amount of exited frequencies) and measurement time and thus depends on the specific research question or assessment goal.

4.2. Application of system identification techniques

This paragraph describes various challenges, limitations, and future perspectives to implement system- identification techniques in a clinical setting.

4.2.1. Assuming time invariance and linear behavior

The system identification techniques assume that human balance control is linear and time invariant (LTI), but in real life, human balance control is highly non-linear and changes over time. With the right experiment and using small disturbance amplitudes, human stance behavior can be assumed linear around the point of equilibrium (upright stance). However, the parts that compose the neuromuscular controller show time-varying behavior, as changing muscle activation is required for various tasks (De Vlugt, Schouten, & van der Helm, 2002; Ludvig, Visser, Giesbrecht, & Kearney, 2011) and postural responses typically adapt or habituate when perturbations have various directions and sizes (Keshner, Allum, & Pfaltz, 1987; Bloem, van Vugt, Beckley, Remler, & Roos, 1998; Klomp *et al.*, 2014). For example, subjects effectively adapt their sway response in a changing environment by down-weighting the unreliable sensory information and up-weighting the other information sources (Goodworth & Peterka, 2012). Other studies (Van Asseldonk et al., 2006) (Boonstra et al., 2014a, 2014b) showed that in stroke and Parkinson’s disease patients, the contribution to balance control of the two legs can be asymmetrical. Putting more weight on the affected leg can alter the controller properties between the legs to remain in an upright stance (Pasma, Boonstra, Campfens, Schouten, & van der Kooij, 2012). Finally, there exist changes over time due to performance limitations, like fatigue.

In model simulations, the LTI behavior is guaranteed, but interpretation of the outcomes in human experiments must be done carefully. In an experiment, the LTI assumption applies to normal subjects using small perturbations applied in the sagittal plane, which somewhat limits the applicability of the model and methods. When a subject changes its balance control response during the course of the experiment, e.g., from responding stiff to slack, this will lead to an inaccuracy in the estimated FRFs (the estimation will be an average of the stiff and slack dynamic behavior). It is therefore important to instruct participants in a standardized way and check linearity and time invariance of the responses.

4.2.2. Challenges

With age and disease (e.g., Parkinson’s disease) specific problems present in multi-segmental balance control. However, a drawback of analyzing a system with two segments is that two perturbations are needed to be able to determine balance control parameters. In this paper we have focused solely on mechanical disturbances, which are often aimed to identify deteriorations in the nervous system part of the control and in the strategies used (ankle or hip strategy). In addition, sensory disturbances can be used to quantify the visual, proprioceptive, and vestibular contributions to maintain standing balance (Peterka, 2002; Jeka et al., 2006; Pasma et al., 2012).

Another aspect that is not captured so far is the influence of deteriorated cognitive control on the balance control behavior, which is especially an issue in stroke survivors, the elderly, and PD patients (Teasdale & Simoneau, 2001; Doumas, a, & Krampe, 2009; Ambrose, Paul, & Hausdorff, 2013; Stijntjes et al., 2015). This effect could be assessed by having participants perform a dual task while maintaining their balance.

4.2.3. Future perspectives to get the methods to the clinic

In our opinion, system identification techniques could add to the currently used repertoire of balance tests in the clinic by providing a quantitative estimate of the balance control system. However, the methods need to be developed further before they can be used. That is, to bring the system- identification method into clinics, it is first necessary to prove clinical usefulness. Hence, the reliability, sensitivity, and specificity of system identification techniques must be determined and compared to existing clinical balance tests. Subsequently, the ultimate proof is to select a random subject from a healthy young population, a healthy elderly population, and a population with a known deterioration of a specific underlying system and apply system identification techniques to determine from which group this subject was selected.

Acceptance of these system identification techniques in the clinical field will be challenging as the frequency response functions (FRF) are not directly related to the mechanisms involved in balance control. The FRF shows the behavior of the system, but does not reveal which physiological mechanisms are underlying

the neuromuscular controller. Hence, by fitting a model to the estimated FRF, the outcome measures are now specific parameters with a physiological meaning and the changes in FRF can be related to changes in e.g. stiffness or time delays. A prerequisite for reliable physiological parameters is a reliable FRF, which is not self-evident as we have shown in this study.

Finally, it needs to be determined whether the proposed methods are more effective than the current clinical practice: Evaluation of cost-effectiveness and long-term benefits for the patient in terms of quality of life should be an inherent part of the evaluation process.

5. Conclusion

System identification is the art and science of building mathematical models of dynamical systems (Ljung, 2010). In this paper we showed the ''science,'' e.g. the basic principles of various system identification techniques and the ''art,'' e.g. system identification techniques aimed at application of multi-segmental and closed-loop balance control. Model simulations showed that non-parametric system identification techniques are favorable over parametric estimates in identification of the neuromuscular controller in standing balance. Both multisine signals and filtered noise signals can be used to estimate these dynamics reliably, in which multisine signals have the advantage to excite specific frequencies of interest and therefore have a better NSR. By this overview of the applicability, advantages and disadvantages of the various currently available system identification techniques, a step is made toward applying system identification techniques to detect age and disease-related changes in balance control.

Acknowledgments

This research is supported by the Dutch Technology Foundation STW (NeuroSIPE #10,737 BalRoom) which is part of the Netherlands Organization for Scientific Research (NWO) and partly funded by the Ministry of Economic Affairs.

Appendix

To validate the MIMO and closed-loop system identification techniques, the underlying mechanisms of standing balance control were described in a model structure. Fig. 1 presents a simplified model of standing balance control, expressed in a plant (i.e. the biomechanics of the human body) and a neuromuscular controller. Each system was described by a mathematical formula (transfer function) with parameters describing the physiology.

Plant: biomechanics of the human body

The rigid body dynamics are represented by a double-inverted pendulum with the sum of corrective joint torques (T_{ank} and T_{hip}) and external force disturbances ($Force_1$ and $Force_2$) as input, and the segment angles (θ_{leg} and θ_{hat}) as output. The equations of motion of this double-inverted pendulum were derived with the TMT method (Koopman, Grootenboer, & Jongh de, 1995). The equations of motion were linearized with a Taylor approximation and rewritten in state space (Boonstra et al., 2013).

Neuromuscular controller: intrinsic feedback

The controller is partly based on intrinsic feedback, describing the muscle and tendon dynamics together with the soft tissue properties. These viscous-elastic properties are modeled by a spring (stiffness K) in series with a damper (D), acting on the states, i.e. the segment angles and angular velocities. Intrinsic properties are sometimes called passive properties. Although the name "passive" suggests otherwise, this feedback mechanism can be modulated by co-activation of antagonistic muscle groups and therefore the parameters of stiffness and damping can vary. The transfer function is described by:

$$H_p = K_p + D_p s \tag{A.1}$$

In which s is the Laplace operator. The ankles and hips were assumed to have different passive properties (H_p^{ank}, H_p^{hip}).

Neuromuscular controller: reflexive feedback

Intrinsic feedback alone is not sufficient to maintain balance. Therefore, the central nervous system (CNS) continuously generates motor commands to compensate for the unstable body dynamics, which is called reflexive feedback control and results in phasic muscle activation. Information to the CNS originates from noisy data (modeled by pink biological noise) from the proprioceptive, visual, and vestibular system.

Reflexive feedback (H_r) was represented by a matrix with stiffness and damping terms, relating the joint torques to the segment angles and angular velocities. This resulted in four transfer functions.

$$\begin{aligned}
H_r^{\theta_{leg}2T_{ank}} &= K_{\theta_{leg}2T_{ank}} + D_{\theta_{leg}2T_{ank}} s \\
H_r^{\theta_{hat}2T_{ank}} &= K_{\theta_{hat}2T_{ank}} + D_{\theta_{hat}2T_{ank}} s \\
H_r^{\theta_{leg}2T_{hip}} &= K_{\theta_{leg}2T_{hip}} + D_{\theta_{leg}2T_{hip}} s \\
H_r^{\theta_{hat}2T_{hip}} &= K_{\theta_{hat}2T_{hip}} + D_{\theta_{hat}2T_{hip}} s
\end{aligned} \tag{A.2}$$

Reflexive control is delayed due to sensory transduction, transmission, and processing, resulting in a lumped time delay (sum of neural conduction time (transport delay), an electromechanical delay (to activate the muscles), and the processing time of sensory information). Furthermore, the conversion from motor control signals to muscle force is represented by the muscle-activation dynamics. The time delay (τ_d) and activation dynamics (H_{act}) can be represented by the following transfer functions:

$$H_{TD} = e^{-\tau_d s} \tag{A.3}$$

$$H_{act} = \frac{\omega^2}{s^2 + 2\beta\omega s + \omega^2} \tag{A.4}$$

with ω and β the natural frequency and relative damping of the muscle activation dynamics. For both the ankle and hip joint, different values were chosen (H_{TD}^{ank}, H_{TD}^{hip}, $H_{act}^{ank} H_{act}^{hip}$).

The entire neuromuscular controller (H_c) can be expressed in four transfer functions:

$$\begin{aligned}
H_{c,\theta_{leg}2T_{ank}} &= \frac{T_{ank}}{\theta_{leg}} = H_p^{ank} + H_r^{\theta_{leg}2T_{ank}} H_{TD}^{ank} H_{act}^{ank} \\
H_{c,\theta_{hat}2T_{ank}} &= \frac{T_{ank}}{\theta_{hat}} = H_r^{\theta_{hat}2T_{ank}} H_{TD}^{ank} H_{act}^{ank} \\
H_{c,\theta_{leg}2T_{hip}} &= \frac{T_{hip}}{\theta_{leg}} = H_r^{\theta_{leg}2T_{hip}} H_{TD}^{hip} H_{act}^{hip} \\
H_{c,\theta_{hat}2T_{hip}} &= \frac{T_{hip}}{\theta_{hat}} = H_p^{hip} + H_r^{\theta_{hat}2T_{hip}} H_{TD}^{hip} H_{act}^{hip}
\end{aligned} \tag{A.5}$$

With

$$H_c = \begin{bmatrix} H_{c,\theta_{leg}2T_{ank}}(f) & H_{c,\theta_{hat}2T_{ank}}(f) \\ H_{c,\theta_{leg}2T_{hip}}(f) & H_{c,\theta_{hat}2T_{hip}}(f) \end{bmatrix} \tag{A.6}$$

Table 3
Parameter settings for the model simulations.

Body parameter value	Lower segment (legs)	Upper segment (hat)
Mass [kg]	20.7	48.0
Length [m]	0.826	–
Height of the CoM above lower end [m]	0.521	0.301
Moment of inertia [kg m^2]	6.57	7.07
Disturbance height relative to CoM [m]	0.4	0.44
Passive feedback		
Intrinsic stiffness [Nm/rad]	286	149
Intrinsic damping [Nms/rad]	65.6	24.8
Active feedback		
Transport delay [s]	0.06	0.04
Angular eigen frequency [rad/s]	9.9	12.1
Damping fraction [-]	1.50	1.65
Neural controller	**K** [Nm/rad]	**D** [Nms/rad]
$\theta_{leg}2T_{ank}$	567.16	236.80
$\theta_{hat}2T_{ank}$	291.82	108.91
$\theta_{leg}2T_{hip}$	153.38	107.08
$\theta_{hat}2T_{hip}$	159.94	105.88

Parameter settings

Parameters for the plant and controller need to be set in order for the model to work (Table 3). Parameters for body segments are mass, length, height of the CoM above the lower end of the segments, and the moment of inertia about the lower end of the segment. When simulating at a multi-segmented model, the equations of motion in the plant are separated for a lower segment (legs) with a torque around the ankle and an upper segment (hat) with a torque around the hip. The two joints have different controller properties; intrinsic properties and also the time delays and activation dynamics were different between the segments. These parameters are described by Kiemel et al. (2011). In all simulations, the data were collected with a sample frequency of 1 kHz.

References

Accornero, N., Capozza, M., Rinalduzzi, S., & Manfredi, G. W. (1997). Clinical multisegmental posturography: age-related changes in stance control. *Electroencephalography and Clinical Neurophysiology, 105*, 213–219.

Ambrose, A. F., Paul, G., & Hausdorff, J. M. (2013). Risk factors for falls among older adults: a review of literature. *Maturitas, 75*, 51–61.

Barin, K. (1989). Evaluation of a generalized model of human postural dynamics and control in the sagittal plane. *Biological Cybernetics, 61*, 37–50.

Berg, K., Wood-Dauphinee, S., Williams, J. I., & Gayton, D. (1989). Measuring balance in the elderly: preliminary development of an instrument. *Physiotherapy Canada, 41*, 304–311.

Bloem, B. R., van Vugt, J., Beckley, D., Remler, M., & Roos, R. (1998). Habituation of lower leg stretch responses in Parkinson's disease. *Electroencephalography and Clinical Neurophysiology, 109*, 73–77.

Boonstra, Ta., Schouten, A. C., van Vugt, J. P. P., Bloem, B. R., & van der Kooij, H. (2014a). Parkinson's disease patients compensate for balance control asymmetry. *The Journal of Neurophysiology, 112*(12).

Boonstra, Ta., van Vugt, J. P. P., van der Kooij, H., & Bloem, B. R. (2014b). Balance asymmetry in Parkinson's disease and its contribution to freezing of gait. *PLoS One, 9*(7), 1–9.

Boonstra, T. A., Schouten, A. C., van der Helm, F. C. T., & van der Kooij, H. (2013). Identification of the contribution of the ankle and hip joints to multi-segmental balance control. *Journal of NeuroEngineering and Rehabilitation, 23*(10), 1–18.

Cohen, H., Heaton, L. G., Congdon, S. L., & Jenkins, H. A. (1996). Changes in sensory organization test scores with age. *Age Aging, 25*, 39–44.

Doumas, M., a, R. M., & Krampe, R. T. (2009). Working memory and postural control: adult age differences in potential for improvement, task priority, and dual tasking. *Journals of Gerontology Series B: Psychological Sciences and Social Sciences, 64*, 193–201.

Engelhart, D., Pasma, J. H., Schouten, A. C., Meskers, C. G. M., Maier, A. B., Mergner, T., & van der Kooij, H. (2014). Impaired standing balance in elderly: a new engineering method helps to unravel causes and effects. *Journal of the American Medical Directors Association, 15*(227), e1–e6.

Engelhart, D., Schouten, A. C., Aarts RGKM, & van der Kooij, H. (2015). Assessment of multi-joint coordination and adaptation in standing balance : a novel device and system identification technique. *IEEE Transactions on Neural Systems and Rehabilitation Engineering, 23*(6), 973–982 doi: Doi 10.1109.

Fujisawa, N., Masuda, T., Inaoka, H., Fukuoka, Y., Ishida, A., & Minamitani, H. (2005). Human standing posture control system depending on adopted strategies. *Medical & Biological Engineering & Computing, 43*, 107–114.

Ganz, D. A., Bao, Y., Shekelle, P. G., & Rubenstein, L. Z. (2007). Will my patient fall? *The Journal of the American Medical Association, 297*, 77–86.

Goodworth, A. D., & Peterka, R. J. (2012). Sensorimotor integration for multisegmental frontal plane balance control in humans. *The Journal of Neurophysiology, 107*, 12–28.

Horak, F. B., & Nashner, L. M. (1986). Central programming of postural movements. *The Journal of Neurophysiology, 55*, 1369–1381.

Hsu, W.-L., Chou, L.-S., & Woollacott, M. (2013). Age-related changes in joint coordination during balance recovery. *Age (Omaha), 35*, 1299–1309.

Jeka, J., Allison, L., Saffer, M., Zhang, Y., Carver, S., & Kiemel, T. (2006). Sensory reweighting with translational visual stimuli in young and elderly adults: the role of state-dependent noise. *Experimental Brain Research, 174*, 517–527.

Jeka, J. J., Allison, L. K., & Kiemel, T. (2010). The dynamics of visual reweighting in healthy and fall-prone older adults. *Journal of Motor Behavior, 42*, 197–208.

Johansson, R., Magnusson, M., a, F. P., & Karlberg, M. (2001). Multi-stimulus multi-response posturography. *[Online]. Mathematical Biosciences, 174*, 41–59 http://www.ncbi.nlm.nih.gov/pubmed/11595256.

Keshner, E., Allum, J., & Pfaltz, C. (1987). Postural coactivation and adaptation in the sway stabilizing responses of normals and patients with bilateral vestibular deficit. *Experimental Brain Research, 69*, 77–92.

Kiemel, T., Zhang, Y., & Jeka, J. J. (2011). Identification of neural feedback for upright stance in humans: stabilization rather than sway minimization. *The Journal of Neuroscience, 31*, 15144–15153.

Kim, S., Atkeson, C. G., & Park, S. (2012). Perturbation dependent selection of postural feedback gain and its scaling. *Journal of Biomechanics, 45*, 1379–1386.

Kim, S., Horak, F. B., Carlson-Kuhta, P., & Park, S. (2009). Postural feedback scaling deficits in Parkinson's disease. *The Journal of Neurophysiology, 102*, 2910–2920.

Kingma, H., Gauchard, G. C., de Waele, C., van Nechel, C., Bisdorff, A., Yelnik, A., Magnusson, M., & Perrin, P. P. (2011). Stocktaking on the development of posturography for clinical use. *The Journal of Vestibular Research, 21*, 117–125.

Klomp, A., de Groot, J. H., de Vlugt, E., Meskers, C. G. M., Arendzen, J. H., & van der Helm, F. C. T. (2014). Perturbation amplitude affects linearly estimated neuromechanical wrist joint properties. *IEEE Transactions on Biomedical Engineering, 61*(4), 1005–1014.

Van Asseldonk, E. H. F., Buurke, J. H., Bloem, B. R., Renzenbrink, G. J., Nene, A. V., van der Helm, F. C. T., & van der Kooij, H. (2006). Disentangling the contribution of the paretic and non-paretic ankle to balance control in stroke patients. *Experimental Neurology, 201*, 441–451.

Van der Kooij, H., van Asseldonk, E., & van der Helm, F. C. T. (2005). Comparison of different methods to identify and quantify balance control. *The Journal of Neuroscience Methods, 145*, 175–203.

Van der Kooij, H., van Asseldonk, E. H. F., Geelen, J., van Vugt, J. P. P., & Bloem, B. R. (2007). Detecting asymmetries in balance control with system identification: first experimental results from Parkinson patients. *Journal of Neural Transmission, 114*, 1333–1337.

Van der Kooij, H., & Peterka, R. J. (2011). Non-linear stimulus-response behavior of the human stance control system is predicted by optimization of a system with sensory and motor noise. *The Journal of Computational Neuroscience, 30*, 759–778.

Van der Kooij, H., & de Vlugt, E. (2007). Postural responses evoked by platform perturbations are dominated by continuous feedback. *The Journal of Neurophysiology, 98*, 730–743.

Koopman, B., Grootenboer, H., & Jongh de, H. (1995). An inverse dynamics model for the analysis, reconstruction and prediction of bipedal walking. *Journal of Biomechanics, 28*, 1369–1376.

Laessoe, U., Hoeck, H. C., Simonsen, O., Sinkjaer, T., & Voigt, M. (2007). Fall risk in an active elderly population-can it be assessed? *Journal of Negative Results in BioMedicine, 6*.
Ljung, L. (1999). *System identification: theory for the user*. Prentice-Hall.
Ljung, L. (2010). Perspectives on system identification. *Annual Reviews in Control, 34*, 1–12.
Ludvig, D., Visser, T. S., Giesbrecht, H., & Kearney, R. E. (2011). Identification of time–varying intrinsic and reflex joint stiffness. *IEEE Transactions on Biomedical Engineering, 58*, 1715–1723.
Mergner, T. (2010). A neurological view on reactive human stance control. *Annual Reviews in Control, 34*, 177–198.
Muir, S. W., Berg, K., Chesworth, B., Klar, N., & Speechley, M. (2010). Quantifying the magnitude of risk for balance impairment on falls in community-dwelling older adults: a systematic review and meta-analysis. *Journal of Clinical Epidemiology, 63*, 389–406.
Park, S., Horak, F. B., & Kuo, A. D. (2004). Postural feedback responses scale with biomechanical constraints in human standing. *Experimental Brain Research, 154*, 417–427.
Pasma, J. H., Boonstra, T. A., Campfens, S. F., Schouten, A. C., & van der Kooij, H. (2012). Sensory reweighting of proprioceptive information of the left and right leg during human balance control. *The Journal of Neurophysiology, 108*, 1138–1148.
Pasma, J. H., Engelhart, D., Schouten, A. C., van der Kooij, H., Maier, A. B., & Meskers, C. G. M. (2014). Impaired standing balance: the clinical need for closing the loop. *Neuroscience, 267C*, 157–165.
Perreault, E. J., Kirsch, R. F., & Acosta, A. M. (1999). Multiple-input , multiple-output system identification for characterization of limb stiffness dynamics. *Biological Cybernetics, 80*, 327–337.
Peterka, R. J. (2002). Sensimotor integration in human postural control. *The Journal of Neurophysiology, 88*, 1097–1118.
Peterka, R. J. (2003). Simplifying the complexities of maintaining balance. *IEEE Engineering in Medicine and Biology Magazine, 22*, 63–68.
Pintelon, R., & Schoukens, J. (2012). *System identification: a frequency domain approach*. John Wiley and Sons.
Rubenstein, L. Z. (2006). Falls in older people: epidemiology, risk factors and strategies for prevention. *Age Ageing, 35*(2), Ii37–ii41.
Sibley, K. M., Straus, S. E., Inness, E. L., Salbach, N. M., & Jaglal, S. B. (2013). Clinical balance assessment: perceptions of commonly-used standardized measures and current practices among physiotherapists in Ontario, Canada. *Implementation Science, 8*, 33.
Speers, R., Kuo, D., & Horak, F. B. (2002). Contributions of altered sensation and feedback responses to changes in coordination of postural control due to aging. *Gait Posture, 16*, 20–30.
Stijntjes, M., Pasma, J. H., Vuuren van, M., Blauw, G. J., Meskers, C. G. M., & Maier, A. B. (2015). Low cognitive status is associated with a lower ability to maintain standing balance in elderly outpatients. *Gerontology, 61*, 124–130.
Teasdale, N., & Simoneau, M. (2001). Attentional demands for postural control: the effects of aging and sensory reintegration. *Gait Posture, 14*, 203–210.
Verhaegen, M. (2007). *Filtering and system identification; a least square approach*. New York: Cambridge University Press.
Visser, J. E., Carpenter, M. G., van der Kooij, H., & Bloem, B. R. (2008). The clinical utility of posturography. *Clinical Neurophysiology, 119*, 2424–2436.
De Vlugt, E., Schouten, A. C., & van der Helm, F. C. T. (2002). Adaptation of reflexive feedback during arm posture to different environments. *Biological Cybernetics, 87*, 10–26.
De Vlugt, E., Schouten, A. C., & van der Helm, F. C. T. (2003). Closed-loop multivariable system identification for the characterization of the dynamic arm compliance using continuous force disturbances: a model study. *The Journal of Neuroscience Methods, 122*, 123–140.
De Vlugt, E., Schouten, A. C., & van der Helm, F. C. T. (2006). Quantification of intrinsic and reflexive properties during multijoint arm posture. *The Journal of Neuroscience Methods, 155*, 328–349.
Van Wingerden, J.-W. (2008).Control of Wind Turbines with “Smart” Rotors: Proof of Concept & LPV Subspace Identification.: 160,
Winter, D. A., Patla, A. E., Rietdyk, S., & Ishac, M. G. (2001). Ankle muscle stiffness in the control of balance during quiet standing. *The Journal of Neurophysiology, 85*, 2630–2633 http://www.ncbi.nlm.nih.gov/pubmed/11387407.

Denise Engelhart received the M.Sc. degree in biomedical engineering from the University of Twente, Enschede, The Netherlands in 2011. In 2015, she obtained her Ph.D. degree at the University of Twente in close collaboration with the Free University, Amsterdam and the Leiden University Medical Centre, Leiden. Her research focuses on using system identification techniques to study and quantify human balance control. Currently she works as a lecturer at the Rotterdam University of Applied Sciences, within the educational program of Healthcare Technology.

Tjitske A. Boonstra received the M.Sc. degree in human movement sciences in 2006 from the VU University, Amsterdam. In 2013, she obtained her Ph.D. degree in biomechanical engineering from the University of Twente. Currently, she is a postdoctoral researcher at the Johns Hopkins University in the USA. Her research focuses on developing new quantitative assessment techniques and methods based on system identification for human balance control. Concurrently, she is applying these new and adopted methods in patients with neurological movement disorders, in order to create more insight into the pathophysiology of these diseases.

Dr. ir. Ronald Aarts (1962) received his Ph.D. degree in Applied Physics from the Eindhoven University of Technology, Eindhoven, the Netherlands, in 1993. He is an Associate Professor at the University of Twente, Enschede, the Netherlands in the Department of Mechanical Automation and Control. His research and teaching interests include Systems and Control, System Identification, (Flexible) Multibody Dynamics and Mechatronics.

Alfred C. Schouten received the MSc and PhD degrees in mechanical engineering from the Delft University of Technology, Delft, the Netherlands, in 1999 and 2004, respectively. He is currently an associate professor at the Delft University of Technology and the University of Twente, Enschede, the Netherlands. He is a co-founder of the Delft Laboratory for Neuromuscular Control. His research interests include the field of neuromuscular control and techniques to quantify the functional contribution of afferent feedback, neuromuscular modeling, haptic manipulators, and system identification. His research focuses on both able-bodied individuals and individuals suffering from movement disorders.

Prof. Dr. ir. Herman van der Kooij, (1970) received his Phd with honors (cum laude) in 2000 and is from 2010 full professor in Biomechatronics and Rehabilitation Technology at the Department of Biomechanical Engineering at the University of Twente (0.8 fte), and Delft University of Technology (0.2fte), the Netherlands. His expertise and interests are in the field of human motor control, adaptation, and learning, rehabilitation robots, diagnostic, and assistive robotics, virtual reality, rehabilitation medicine, and neuro-computational modeling He was awarded the prestigious personal Dutch VIDI and VICI grants in 2001 and 2015 respectively. He is associate editor of IEEE TBME and IEEE Robotics and Automation Letters, member of IEEE EMBS technical committee of Biorobotics, and was member of several scientific program committees in the field of rehabilitation robotics, bio robotics, and assistive devices